DIELECTRIC-SPECTROSCOPY APPLICATIONS WHILE DRILLING IN THE VACA MUERTA FORMATION

Scott J. Jacobsen[1], Eric Decoster[1], James Hemingway[1], Frank Shray[1], Barbara I. Anderson[1], Peter R. Swinburne[1]

1: NoHiddenPay, LLC. sj@nohiddenpay.com, ed@nohiddenpay.com, jh@nohiddenpay.com, fs@nohiddenpay.com, ba@nohiddendpay.com, ps@nohiddendpay.com

Keywords: Dielectric, Spectroscopy, Dispersion, Vaca Muerta, Permittivity, Conductivity, Wideband, Modeling, Propagation, Electromagnetic, Phase-shift, Attenuation, Anisotropic, Resistivity, Unconventional

RESUMEN

Los perfiles de flujo de producción en una mayoría de pozos laterales no convencionales siguen mostrando a menudo un comportamiento ineficiente. Las tasas de flujo de gas o líquidos pueden variar sorprendentemente de una etapa a otra e incluso de un grupo a otro en los pozos de drenaje, que se supone que se perforan y se completan en una zona productiva homogénea desde el talón hasta la punta. Los pozos laterales de producción, que penetran en intervalos cada vez más largos del reservorio objetivo, rara vez disponen de datos petrofísicos más amplios que una simple medición de GR cerca del pozo. Por lo tanto, con el aumento de la distancia horizontal desde el pozo piloto, suponer que la formación objetivo sea direccionalmente homogénea se vuelve progresivamente menos confiable. Y con una evaluación limitada de las variaciones de las propiedades del reservorio en la región cercana al pozo a lo largo de la trayectoria horizontal, la acción correctiva se vuelve difícil.
En la formación de Vaca Muerta, las prácticas de perforación y completación de pozos han logrado un enorme progreso en cuanto a rentabilidad. Se pueden lograr más mejoras mediante una descripción más completa de las propiedades de la formación durante la perforacion del pozo horizontal
Hemos implementado un modelo mecanístico recientemente publicado que describe los fenómenos EM de banda ancha en las formaciones geologicas. El análisis petrofísico de los perfiles de campo se introduce para simular los perfiles de permitividad y conductividad dieléctrica a varias frecuencias de la herramienta de perfilaje. Para investigar la relación entre las propiedades de la formación de Vaca Muerta y la respuesta EM asociada a estas propiedades, se ha construido una sección vertical compuesta del reservorio utilizando datos petrofísicos típicos. El modelo se utilizó para simular las trayectorias de los pozos a través de esta sección y las respectivas curvas de permitividad dieléctrica y conductividad que resultarían al perforar con herramientas típicas de resistividad LWD.
También estamos finalizando las pruebas de campo de un proceso neutral para invertir directamente los datos de atenuación y cambio de fase medidos a partir de la adquisición de herramientas de resistividad LWD para obtener la conductividad y la permitividad de la formación. El algoritmo se desarrolló de nuevo a partir de un trabajo publicado anteriormente, reimplementando la solución de las ecuaciones de Maxwell de una manera más eficiente desde el punto de vista computacional. La inversión proporciona curvas de perfil de conductividad/resistividad independientes y curvas de perfil de permitividad a las distintas frecuencias de la herramienta LWD utilizadas.
Este estudio implementa tanto la nueva simulación predictiva como el nuevo algoritmo de inversión LWD. Estos dos algoritmos son complementários y relacionan conductividad y permitividad con las propiedades clave del yacimiento. Los resultados son coherentes: la simulación predictiva seguida de la inversión reproducen de manera confiable los datos originales de entrada y viceversa. La inversión LWD se ha probado con datos de pozos piloto, pozos de producción de alto ángulo y laterales para obtener una nueva visión del yacimiento y ayudar a optimizar las trayectorias horizontales en intervalos más largos.

INTRODUCTION

The Vaca-Muerta field has traditionally been characterized using mostly vertical or mildly deviated wells. They have only been logged with Wireline for formation evaluation and petrophysical analysis. The combination of array induction tools and multi-frequency dielectric tools have provided a first insight regarding the water saturation and salinity distribution across the field. The frequency spectrum of these electromagnetic measurements covers five orders of magnitude from the tens of kHz for induction tools to the low-GHz range for the dielectric tools. However, these measurements do not operate in the high-100-kHz and low-MHz range. Thus, the dispersion study appears to be incomplete, having a severe blind spot in this intermediate frequency range.

Despite a general assumption that unconventional source rock reservoirs are laterally quite homogeneous in reservoir qualities from heel to toe in most producing lateral wells, advanced production log analysis continually shows a great deal of stage-to-stage and even perforation cluster-to-cluster flow performance variation (Chadwick and Whittaker, 2001). Figures 1a,b show a very long lateral production drainhole well drilled in an unconventional reservoir, Well #1. This was completed and put on production without the benefit of any formation evaluation to guide the completion design. The only data acquired was a gamma ray log, shown in the middle track of the figure, which responds mainly to the uranium content of the formation and has little to no relationship to the transport properties of the rock which control the flow of hydrocarbon fluids. The well trajectory seen in the lower track illustrates a successful geo-steering operation as the well is completely within the target reservoir. The upper track shows the production profile in terms of gas flow per frac stage, which was determined after the well was on stable flow several months after being put on line.

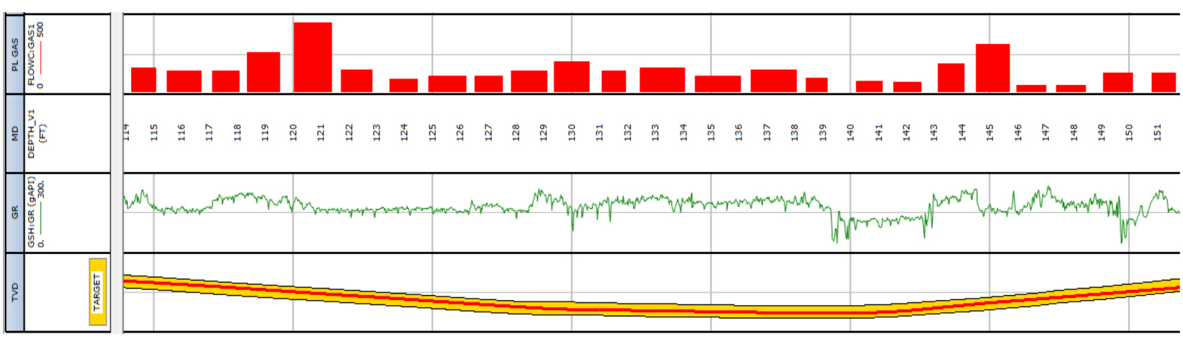

Figure 2a. Lateral production drainhole in an unconventional shale gas reservoir. Track 1 is the well trajectory in TVD (red curve); yellow shading is the target window. Track 2 is the GR, the only petrophysical data acquired. Track 3 is measured depth in feet. Track 4 is gas production per stage in BOEPD.

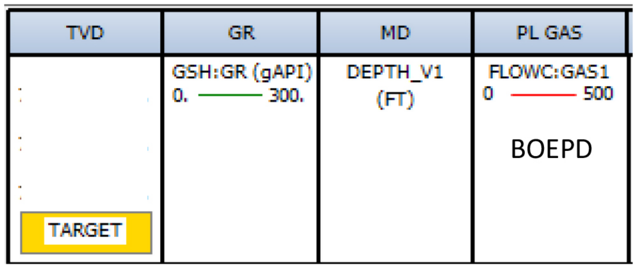

Figure 2b. Curve header insert detail for figure 1a.

A reasonable interpretation of the disparate and sub-optimal production behavior among the various stages is that there is more formation lateral heterogeneity than appreciated, despite the successful geosteering and drilling to keep the wellbore in the reservoir "sweet spot". This would hold potentially not only for the vertical curtain section through which the lateral trajectory proceeds, but also for the adjoining and parallel wells even closely spaced within the pad/lease. Yet for obvious economic reasons, only minimal LWD data is routinely acquired to assess if completion strategies might be improved with a better appreciation of the reservoir over the length of the completed lateral. Perhaps, as above, legacy same-pad pilot hole/production lateral data sets, if any LWD resistivity logging had been done, could be re-examined and the LWD propagation resistivity data inverted for electromagnetic (EM) formation properties. This would seed EM model simulations at both the ends of the dispersion spectrum and could be tied in to EM simulations based on the pilot hole WL data. There may be learnings obtained from comparing wideband dispersion trends to both production and well placement information that could influence future laterals' geosteering planning and/or completion designs.

Our focus is on the application of a dielectric inversion of data from LWD tools to determine EM formation properties of permittivity and conductivity, at up to two typical frequencies, to help solve current volumetric analysis challenges. Also, we keep in mind how this contrasts with taking on the same challenges with appropriate wireline (WL) tool measurements.

There is always a time frame in which the answers must be delivered, usually driven by driven by drilling cycle economics and the need for efficiencies. As LWD technology has evolved, there is a general consensus that basic resistivity and nuclear log measurements LWD are sufficiently accurate to warrant foregoing WL logging, especially in the more expensive offshore and difficult logging conditions operations. In this context there is a motivation to migrate or adapt heretofore WL- exclusive solutions to LWD measurements as applicable: the sooner the petrophysical answers are delivered, the better, in all cases.

Near-wellbore effects on WL tools have been treated extensively with shallow compensation hardware and software processes, both for the effects of hole rugosity and fluid invasion. There is no one compensation method that fits all tools and environments. So a corollary to timely answer delivery early in the drilling cycle is that measurements made quickly after the bit penetrates the formation will generally see much shallower to no filtrate invasion, as this is a relatively slow process. The hole may also be better in gauge/less rugose. The concept is that is always better to avoid the need for measurement compensation altogether.

Fundamental petroleum economics revolves around resource-in-place calculations, based on water saturation analysis from log data. It is also fundamental that water salinity values - in situ in time and place when and where the log measurements are made - are more often than not poorly know in most reservoirs in the world.

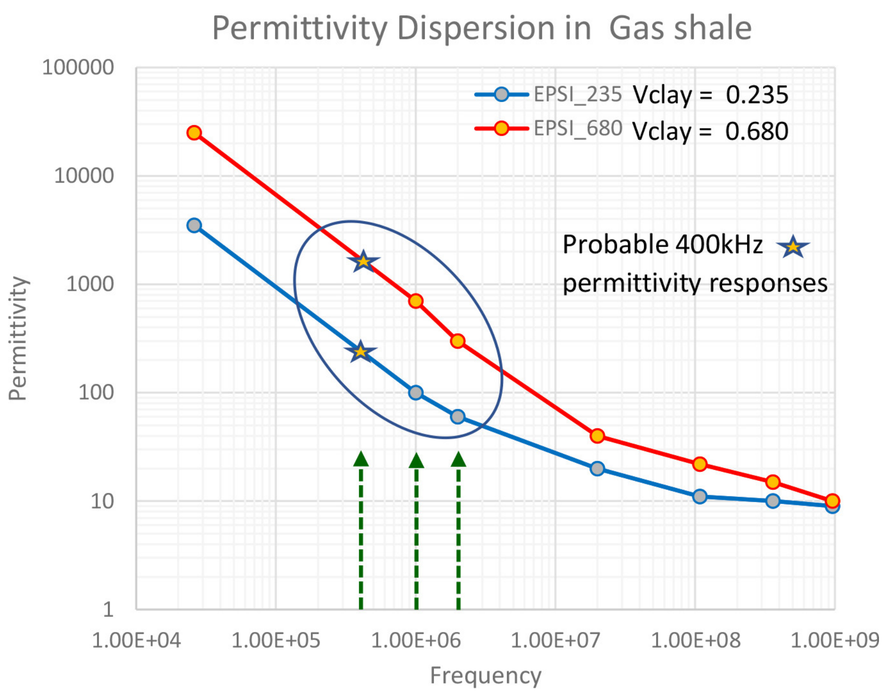

Figure 2. Wideband dielectric dispersion as seen by three EM tools in a North Sea gas shale: induction, LWD, array dielectric. Sensitivity to clay volume is seen at two points as different characteristic dispersion shape. Green arrows show LWD tool frequencies. (Adapted from Wang and Poppitt, 2013)

This is true in all phases of asset development, from exploration to brown field situations. In fact it may be more important in mature fields to know exactly how much remaining hydrocarbon is in place for proper estimation of the value of secondary recovery operations. It is better from a petrophysical stand-point to not to have to rely on Rw in resistivity based saturation models and determine water-filled porosity by another means. This points to the utilization of the water volume sensitivity of the dielectric permittivity of formations, at appropriate frequencies where the water salinity sensitivity is very low. WL dielectric tool measurement applications are grounded on this physics. We seek to take advantage of similar physics with LWD devices.

Clay is omnipresent in all unconventional reservoir formations. Petrophysically the effect on the fluid saturation and thus resource-in-place calculation chain must be accounted for, in terms of both volume fraction of the various clay minerals and their particular electrical properties such as cation exchange capacity (CEC). Knowledge of clay types can often be important in completion design. Clay particle grain size, shape, and specific surface impact reservoir fluid relative permeabilities. This is another area where the impact clay parameters on electrical polarization phenomena in formations can be exploited by studying EM dispersion across certain frequency bands. It may be that adding EM properties at typical LWD frequencies and incorporating these with EM inversions from both WL array induction inversion at the low-frequency side of the dispersion range, and with EM data from WL dielectric tools for the high-frequency side, will provide a relatively well-sampled dispersion characterization of reservoirs. Figure 2 is adapted from Wang and Poppit (2013). It highlights the concept of using wideband EM dispersion from a rich set of WL and LWD tools combined to investigate dispersion behavior related to clay volume and CEC in a North Sea unconventional gas shale reservoir. We also point to excellent work in this key area by Stalheim (2019) who devised a process to take LWD field logs and reverse out the measured phase and attenuation signal data. He subsequently inverted these for EM properties. Illfelder *et al.* (2008) presented work where clay and fluid properties were identified from LWD data inverted for EM properties in both clean and shaly formations.

Norbisrath *et al.* (2017) investigated lower-frequency complex resistivity spectra in Vaca Muerta formations for reservoir parameters controlling production, and they did see increasing sensitivities at frequencies approaching LWD values in some of their experiments. And we encourage the petrophysical community to search out appropriate data sets for joint EM inversion opportunities as clay is a major influencer on EM properties across the entire WL-LWD tool frequency range

At the high frequencies of WL dielectric tools, there is a large dependence of the EM response on solid grain shapes and orientation to the electric field generated by the tool. Early applications of the first WL dielectric tool in the industry, the EPT, were found to yield significantly improved reservoir saturations and completion decisions. (Rasmus and Kenyon, 1981). Physical structure of the formation – especially in carbonates - from meso- to micro-scales is described as rock texture or fabric. This relates to formation resistivity factor but is a broader description, and quantification of which has implications for reservoir fluid flow. Critical dynamic properties of productive formations in the whole permeability/wettability/relative mobility determination task are governed by rock texture. Hydraulic fracturing design also can hinge on determining the texture of the rock in the intervals to be treated.

Pioneering work was done by Norbisrath (2018) who derived dispersion characteristics from high-frequency array dielectric log data, and developed a hydraulic permeability algorithm. This dovetails nicely with the work done by the aforementioned authors in the clay discussion section above to produce EM wideband dispersion evidence from rich data sets (legacy, recent, or planned) and to apply the findings to the large range of formation evaluation problems outlined above.

METHODOLOGY

We first refer the reader to Figure 3. This is a generic diagram of the electromagnetic (EM) response of earth formations over the operating frequency range of typical WL and LWD logging tools. The various polarization phenomena are shown above the curves. The Y axis shows the two main EM properties derived from the tools and output as log curves. The EM conductivity property ("s") is inverted to become the typical resistivity log curve. The EM permittivity property ("   ") is the permittivity curve produced by "dielectric" logging tools that sense EM propagation polarization effects at high frequencies. The critical feature seen in the graph is the frequency dispersion of both properties, that the dispersion is in opposite directions for each, and that permittivity dispersion is more highly pronounced (permittivity is on a logarithmic scale) across the range. We investigate how utilization of the whole wideband permittivity dispersion characteristic might contribute to better completions in unconventional laterals in the Vaca Muerta with a methodology comprised of three steps.

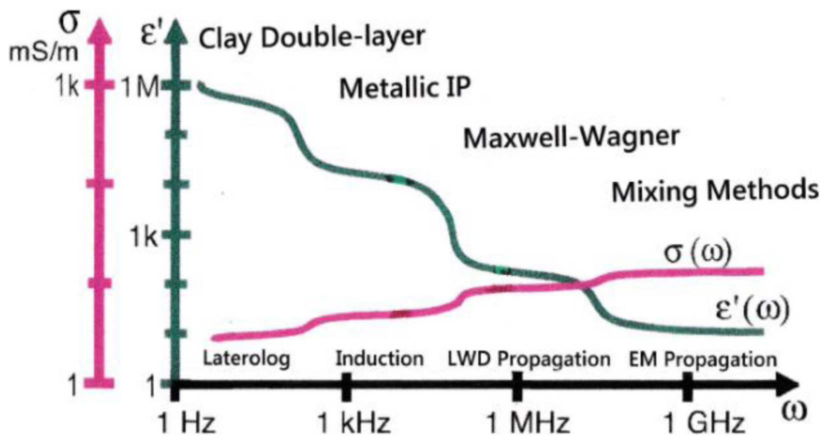

Figure 3. Electromagnetic (EM) response of earth formations over the operating frequency range of typical WL and LWD logging tools. (After Anderson *et al.*, 2022)

The first is to employ a physics-based "geo-electromagnetic" EM model to predict formation permittivity and conductivity properties for the entire frequency range of resistivity devices commonly used. These predictions are based on petrophysical volumetric analysis inputs. We validate the predictions first at high frequencies against permittivity and conductivity outputs from WL array dielectric tool log data, in suitable example wells.

The second step is to validate the PS model at the low end of the frequency range against available induction tool data. As typical induction tools do not generate permittivity outputs, we must first do a dielectric inversion of the fundamental in-phase and quadrature raw tool signal data. We perform point by point dielectric inversions for formation permittivity and conductivity at induction frequencies.

The third step is to complete the dispersion spectrum and validate the PS model in the LWD tool frequency band. This utilizes a recently updated dielectric properties inversion process that has been recently optimized for typical axisymmetric LWD resistivity tools – from any vendor, This step provides for a large amount of field data in many wells, furnishing dielectric permittivity and conductivity formation properties in this frequency range.

With a validated and acceptably accurate geo-electromagnetic model implemented, we can then take Vaca Muerta formation properties from petrophysical volumetric analyses and simulate the new dielectric permittivities and conductivities that would be obtained from inversion of actual field LWD log data.

Step 1 – Wideband Dielectric Property Modeling, High-Frequency Validation

We have chosen at this point to implement a wideband geoelectromagnetic model (the "PS" model) developed and published by Jin and Misra (2020) to predict permittivity and conductivity formation properties at frequencies ranging from 10 Hz to 1 GHz This effective medium model is composed of up to five materials as spherical inclusions – three non-conductive and two conductive, in a host medium of water with varying salinity. Two of the non-conductive inclusions representing the formation volumes are mineral grains such as quartz, feldspars, micas, carbonates, evaporites, etc., with small surface charge, and clay mineral grains with typically much larger surface charge, to a host medium of water with varying salinity. A third non-conductive inclusion is the volume of hydrocarbon. The two conductive spherical inclusions are the minerals pyrite and graphite. The wideband specification is intended to cover the range of typical EM logging tools, as described in Anderson *et al.*, 2007.

In our implementation, as described in Jacobsen, Decoster, *et al.* (2022a), petrophysical analysis mineral volume fractions as log outputs are the inputs to the model, along with the associated mineral and fluid parameters seen in the table. The model is constructed such that one minus the sum of the mineral volume fractions is equal to the water-filled volume fraction (water-filled porosity). The water salinity and diffusion coefficient parameters are applied to this quantity. If hydrocarbon is included in the model, it is considered in the same class as a mineral inclusion, with associated electrical parameters, and serves to further reduce the water-filled volume fraction.

The frequency input is swept from low to high at discrete frequencies of interest involving typical EM logging tools. These are 10, 75, 270, 1k, 26k, 52k, 400k, 500k, 2M, 20M, 108M, 360M, and 960M Hz, and permittivity and conductivity curves are generated at these frequencies. Thus we simulate the EM properties that the tool measurements would be sensitive to at these frequencies. Table 1 lists the main parameter inputs to the model.

Parameter	Units	Range
Frequency	Hz	10^1 to 10^9
Mineral volume fraction	v/v	0 - 1
Mineral relative permittivity		4 to 20
Mineral spherical grain radius	m	1 x10^{-3} to 5 x10^{-7}
Conductive mineral conductivity	S/m	1000 to 500
Conductive mineral diffusion coefficient	m^2/s	5 x10^{-5}
Non-conductive mineral surface conductance	S	1 x 10^{-9} to 1 x 10^{-7}
Water salinity	S/m	1 to 50
Water diffusion coefficient	m^2/s	1 x 10^{-9}

Table 1. PS Model Inputs and Parameters

We have used this model to investigate the sensitivity of the 2MHz permittivity to both water-filled porosity and water salinity and quantify the deleterious effects of increasing formation clay volume fraction. We built a synthetic step property formation to vary salinity, water-filled porosity, and clay fractions in various combinations to study the feasibility of deriving a salinity-independent water free porosity interpretation process. The intent was to expand on the work done by Zhang *et al.*, 2021, and support the “dielectric porosity” application for fresh and unknown water salinities to be delivered from LWD measurements, in early time in the drilling process. (Anderson *et al.*, 2022; Jacobsen, Decoster, *et al.*, 2022).

The PS model is well validated by laboratory experiments. (Misra *et al.*, 2016). We are confident to use it to simulate wideband permittivity and conductivity curves based on the several publications that support this. Moreover, if the proper log data sets are available, our implementation allows validation against downhole measurements from logging tools across the same wideband frequency range. We will demonstrate this using an example, Well #2, in figure 4,with an extensive set of wireline data types. This example well is not in Vaca Muerta source rock specifically but penetrates formations with complex lithologies: unconventional clastics and carbonates. It is vertical and was drilled with fresh water-based mud. The wireline log data included array induction, geochemical, nuclear, NMR, and array dielectric tool (“ADT”) measurements. A petrophysical volumetric analysis using this data provides the main log inputs for the mineral volumes and their respective permittivity parameters required by the model.

The model validation process is to simulate permittivity and conductivity curves at the two highest (generally most accurate) array dielectric tool frequencies and to compare the simulated curves to the actual tool data. Figure 4 shows a section of the logged interval with a wide range of both lithologies and porosities.

To effect the reconstruction we potentially adjust both input formation volumes by modifying the petrophysical analysis, and by deviating the input formation properties from their nominal values seen in Table 1. Special attention is needed to carefully tune the clay spherical grain radius, the clay surface conductance, and the host water salinity values. After several manual iterations of these adjustments, we eventually see very good reconciliation of the actual high-frequency ADT permittivities and conductivities and the same curves from the PS model simulation at those frequencies. Similar results were seen with other case example wells with similar data sets, and in a wide range of formations.

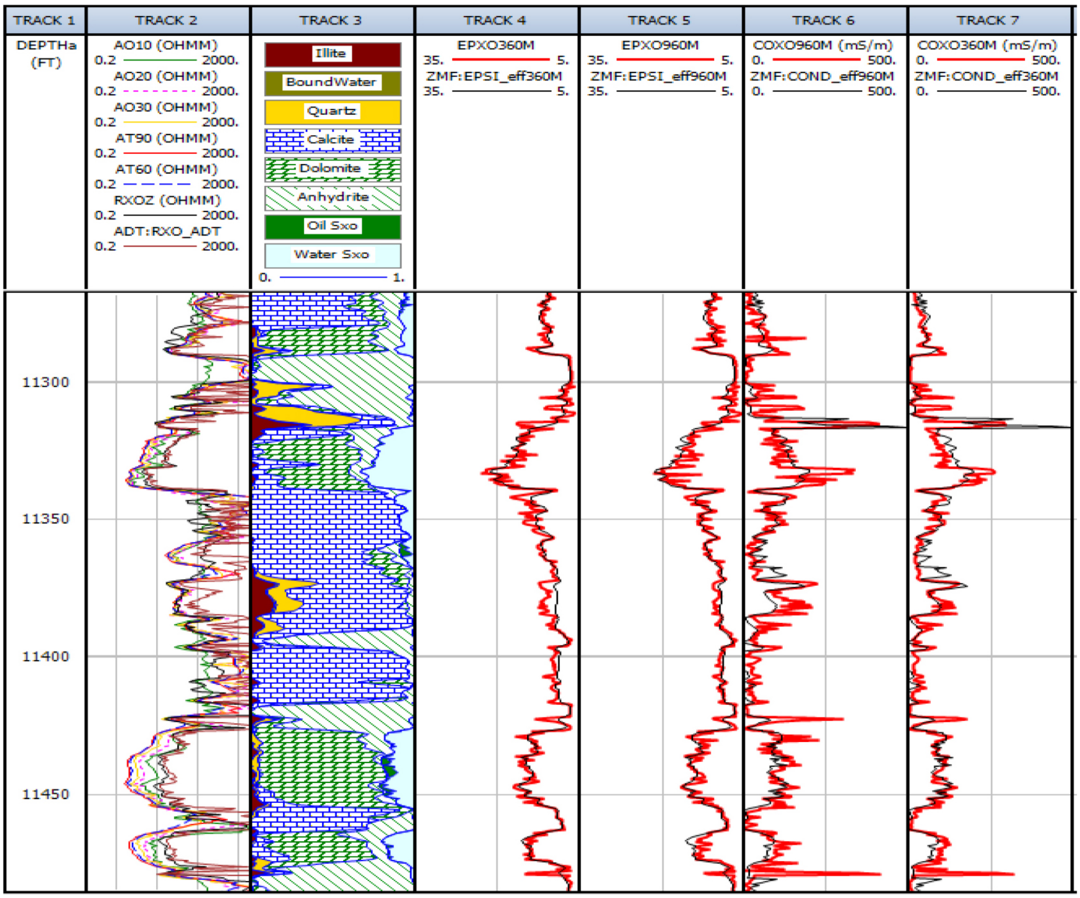

Figure 4. Well #2. Track 2 displays the array induction AT90 and micro-spherically focused log RXOZ curves with shading where mud invasion is interpreted. Track 3 is the volumetric analysis: limestone, dolomite, anhydrite, clay, quartz, and feldspar minerals are seen, with mostly water-filled porosity ranging from almost 0% up to 17% in a mostly dolomite zone. Tracks 4 and 5 each show the actual array dielectric and the PS model simulated permittivity at 360 MHz and 960 MHz respectively. Similarly, Tracks 6 and 7 show the same for the actual and modeled conductivity curves.

Step 2 – Wideband Dielectric Property Modeling, Validation via Dielectric Inversion of Induction Data

Wireline array-induction tools usually serve to provide the formation resistivity or conductivity. They are radially deep-reading instruments, which illuminate the formation beyond the invasion front, provide a radial resistivity or conductivity profile and therefrom generate a water-saturation profile. The relationship between measured formation conductivity and estimated water saturation is at the core of petrophysics. The induction- measurement concept assumes negligible dielectric effects and then provides a signal, which to lowest order is directly proportional to the formation conductivity. However, lowest order proves to be not valid in more conductive formations, where the skin effect causes major distortions.

Modern array-induction tools consists of basic three-coil building blocks with a single transmitter, which is common to all array measurements, and a pair of receivers for each channel. The transmitter and the two receivers all constitute solenoidal coils, which may be approximated as magnetic dipoles. The two receivers have different magnetic-dipole moments, which are designed-dimensioned so that for their distances from thetransmitter the directly coupled transmitter signal is cancelled to a high degree of accuracy. The receivers measure the difference of the electromagnetic signals from the oscillating transmitter both in phase with the transmitter as R-signal and in quadrature (90°) against the transmitter as X-signal. The quadrature or X-signal offers a first-order correction to the R-signal, which mostly compensates for the skin-effect distortion.

The induction-measurement concept assumes negligible dielectric effects. Induction tools operate at comparatively low frequencies in the tens of kHz. Maxwell-Ampère's equation combines electric conductivity σ and dielectric permittivity ε to a single, complex-valued quantity: the complex dielectric constant ε^* or the complex electric conductivity σ^*:

$$\varepsilon^* = \varepsilon + i\frac{\sigma}{\omega} \Leftrightarrow \sigma^* = \sigma - i\omega\varepsilon \qquad (1)$$

Here ω is the circular frequency $\omega = 2\pi f$. The dielectric permittivity ε is the product of the absolute permittivity of vacuum ε_0 ($\cong 8.8542*10^{-12}$ As/Vm) and the dimensionless relative dielectric permittivity ε_r. The product $\omega\varepsilon_0$ gives a conductivity, which at 25 kHz is about $\omega\varepsilon_0 \cong 1.4$ μS/m. This value is three orders of magnitude below the lower end of the induction-measurement range of 1 mS/m. The assumption of negligible dielectric effects seems reasonable, but may not always be valid (Anderson *et al.* 2006 & 2008). Most rock formations render dielectric-permittivity effects at induction frequencies invisible; however, some formations, especially source-rock shales with high hydrocarbon content, show relative dielectric permittivities ε_r in excess of 10,000 (Altman *et al.* 2008, Anderson *et al.* 2008, Misra *et al.* 2016). In these formations dielectric effects are no longer negligible.

These large dielectric effects may be extracted from the combined R- and X-signals of the array induction tools. These R- and X-signals are orthogonal; they are 90° out of phase. Thus they are real and imaginary part of a complex-valued signal. This complex-valued signal is a complex function of the complex conductivity σ^* (or complex dielectric constant ε^*). The presence of the non-negligible dielectric permittivity skews the phase alignment of the received signal against the transmitter source signal (Anderson *et al.* 2008). However, the combined R-X-signal may be uniquely inverted for the complex conductivity σ^* (Lüling 2015). This inversion algorithm has

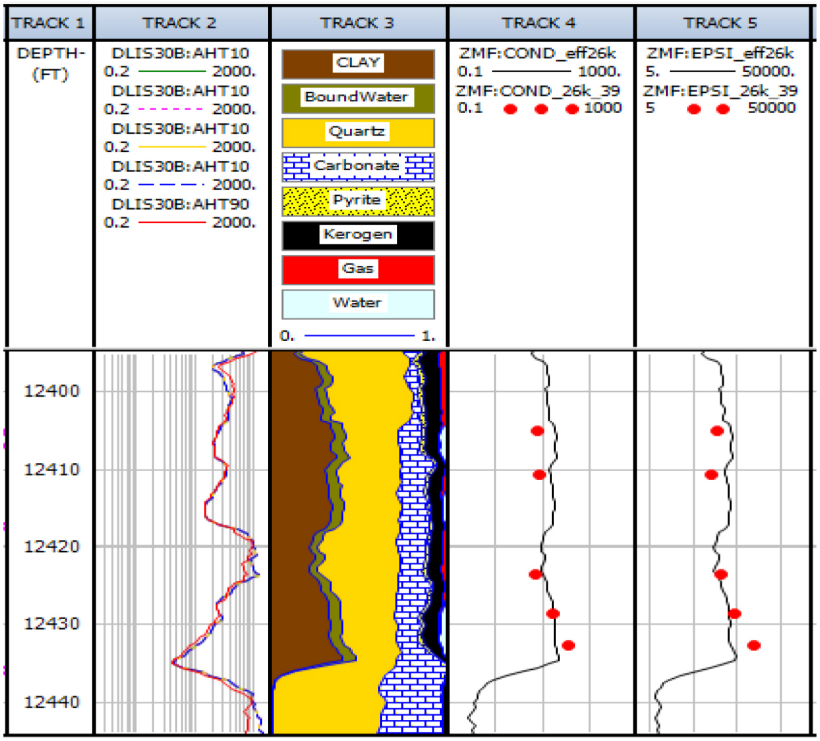

Figure 5. Well #3. Unconventional North American gas shale reservoir. It is vertical and was drilled with fresh water-based mud. Track 2: array induction curves. Track 3: volumetric analysis. Tracks 4, 5: Inversion of 39" induction array data for 26 kHz permittivity and conductivity at select depth points, respectively, red symbols; simulation of associated 26 kHz quantities from dielectric property modeling, black curves.

been redeveloped, improved, and refined; then it has been applied to several array-induction logs, showing a rich plethora of phenomena entering into petrophysics.

This dielectric-inversion algorithm has been applied to multi-frequency array-induction tools. The results show electric conductivities σ, which are fairly stable over the frequency range. On the other hand, the inverted dielectric permittivities ε vary considerably with frequency; this variation with frequency is called dispersion. In all cases the inverted permittivity diminishes with increasing frequency. It may be around 30,000 at 25 kHz and decrease to around 20,000 at 50 kHz. Thus the dispersion is monotonically decreasing with frequency, but decreasing weaklier than a direct proportionality.

Here we proceed with the PS model validation process by simulating permittivity and conductivity curves at the induction tool frequency of 26 kHz. Inversion of the actual tool data for the EM properties was done using the 39" array signals, as these have been determined to be the most stable compared to the other acquired arrays (Anderson *et al.* 2006), and this was performed on a point-by-point basis. Figure 5 is from Well #3, a North American gas shale reservoir vertical pilot hole. The figure shows a logged section of the productive reservoir containing typical quantities of clay, quartz, carbonate, pyrite, and kerogen, with gas and water. PS model adjustments are iterated as described above for the high-frequency simulations, and we again see very good reconciliation of the actual induction-frequency permittivities and conductivities and the same curves from the PS model simulation at that frequency.

Similar results were seen with other case example wells with similar data sets, and in a wide range of formations. We argue from these test results that the PS model is successful in predicting both the low frequency induction tool and high frequency dielectric tool permittivity and conductivity values from petrophysical analysis. This thus lends credence to the simulation of formation dielectric properties at LWD tool frequencies.

Step 3 – Wideband Dielectric Property Modeling, Validation via Dielectric Inversion of LWD Data

Logging While Drilling (LWD) mostly uses electromagnetic propagation-resistivity measurements for formation resistivity and hence water saturation. Today's propagation-resistivity tools are array tools with several transmitters around a pair of receivers. These tools emit radio waves at two operating frequencies in the mid- 100-kHz to low-MHz range and measure the attenuation AT and phase shift PS between the two receivers. The measurements are based on Maxwell's electrodynamics, where electric conductivity and dielectric permittivity are combined to a single, complex-valued dielectric constant. At the fairly low operating frequencies, dielectric effects are expected to be small; hence the measurement depends mostly on conductivity (or resistivity). Therefore, the tools routinely provide two apparent resistivities R_{AT} and R_{PS}. The dielectric permittivity is substituted by an estimate, which is a function of conductivity and varies among the service providers.

The assumption of small dielectric effects may not always be valid. In fact, Anderson *et al.* (2007) showed some examples of large dielectric effects in source shales. In this situation it is more appropriate to simultaneously invert the attenuation and phase shift to apparent dielectric permittivity and electric conductivity (Lüling, 2015). In fact, attenuation and phase shift constitute real and imaginary part of the complex-valued signal ratio of the two receiver signals. This complex-valued ratio thus is a function of the complex dielectric constant; it even is a holomorphic function. This function is separately inverted for each operating frequency (Anderson *et al.*, 2022). The inversion is performed for each log station; it assumes a homogeneous and isotropic medium. It also assumes that the LWD data have been borehole corrected.

The log examples with inverted dielectric permittivities frequently show apparent permittivities ε_a that considerably vary between the mid-100-kHz and the low-MHz range. The dielectric permittivity is dispersive, it diminishes with increasing frequency. Thus, the dielectric permittivity and its dispersion provide two new petrophysical measurements. The present study investigates the role that permittivity and its dispersion may play in an estimation of water-filled porosity.

The dielectric inversion of the multi-frequency electromagnetic measurements applies to all propagation- resistivity array tools. The current version is limited to axisymmetric tools, whose apparent resistivity data R_{AT} and R_{PS} from the logs are reverse-converted back to attenuation AT and phase shift PS with the vendor- specific dielectric estimate. The (AT, PS) pair for each transmitter spacing and every operating frequency are then inverted for the apparent complex dielectric constant or the apparent conductivity-permittivity pair (σ_a, ε_a). The only information needed for this task is the tool-array description with its operating frequencies and the dielectric-estimate relationship.

The Society of Petrophysicists and Well-Log Analysts (SPWLA) features a Special-Interest Group (SIG) on Resistivity. This Resistivity SIG regularly provides a catalogue of LWD resistivity tools from all active service providers. The catalogue describes the propagation-resistivity array tools together with their vendor-specific estimates for the dielectric permittivity at the tool-specific operating frequencies. This catalogue serves to convert the tool-specific apparent attenuation and phase-shift resistivities from field logs to basic tool data for further inversion processing.

The LWD propagation-resistivity tools from this SPWLA Resistivity SIG catalogue are approximated as array of axially aligned magnetic point-dipole radiator transmitter and receivers. Such point-dipole radiators offer close-form solutions in a homogeneous medium with given electric conductivity and dielectric permittivity. This close-form solution in turn serves in an iterative inversion algorithm to extract the electric conductivity and dielectric permittivity from the equivalent point-dipole attenuations AT and phase-shifts PS of the various tools (Lüling 2015). This inversion from point-dipole phase-shifts PS and attenuations AT to apparent electric conductivity and dielectric permittivity is a rapidly converging iterative algorithm. This algorithm uses the powerful mathematical tools of complex-function analysis. Usually it achieves convergence in three to five iterations to better that a part in 10^{10}. However, if the formation under investigation features additional petrophysical properties, such as anisotropy or proximity to high-contrast bed boundaries, the algorithm may not converge. In this case, the algorithm is terminated after ten iterations, providing a log-quality-control flag, which indicates that the mathematical and physical assumptions of the inversion algorithms may not be valid and must be generalized to anisotropic media or media with high-contrast stratifications.

During our field test of the LWD Dielectric Inversion LWD data from several different vendors was processed on 20+ wells to date. The types of reservoirs logged include both conventional and unconventional, with vertical to high-angle well trajectories.

In our entire model validation discussion we must also note that at this point that we are not convolving PS model generated permittivity and conductivity properties with any given tool's spatial response function. So we are not simulating the actual tool response curves per se. However for measurements whose spatial response is close to that of the nuclear tool measurements included in the petrophysical volumetric analysis, the simulated and actual EM property curves can often reconstruct quite well. With a high vertical resolution tool such as an array dielectric device, and when the borehole conditions are benign, we see this, in many intervals in the examples so far. We are about to illustrate simulations from the PS model with and comparisons with outputs from our dielectric inversion process and of course the same caveats apply. In the typical LWD logging environments in deviated and high angle wells, we also have to consider in our comparisons the possible perturbing factors on the curves of high relative borehole-bedding plane angles and high

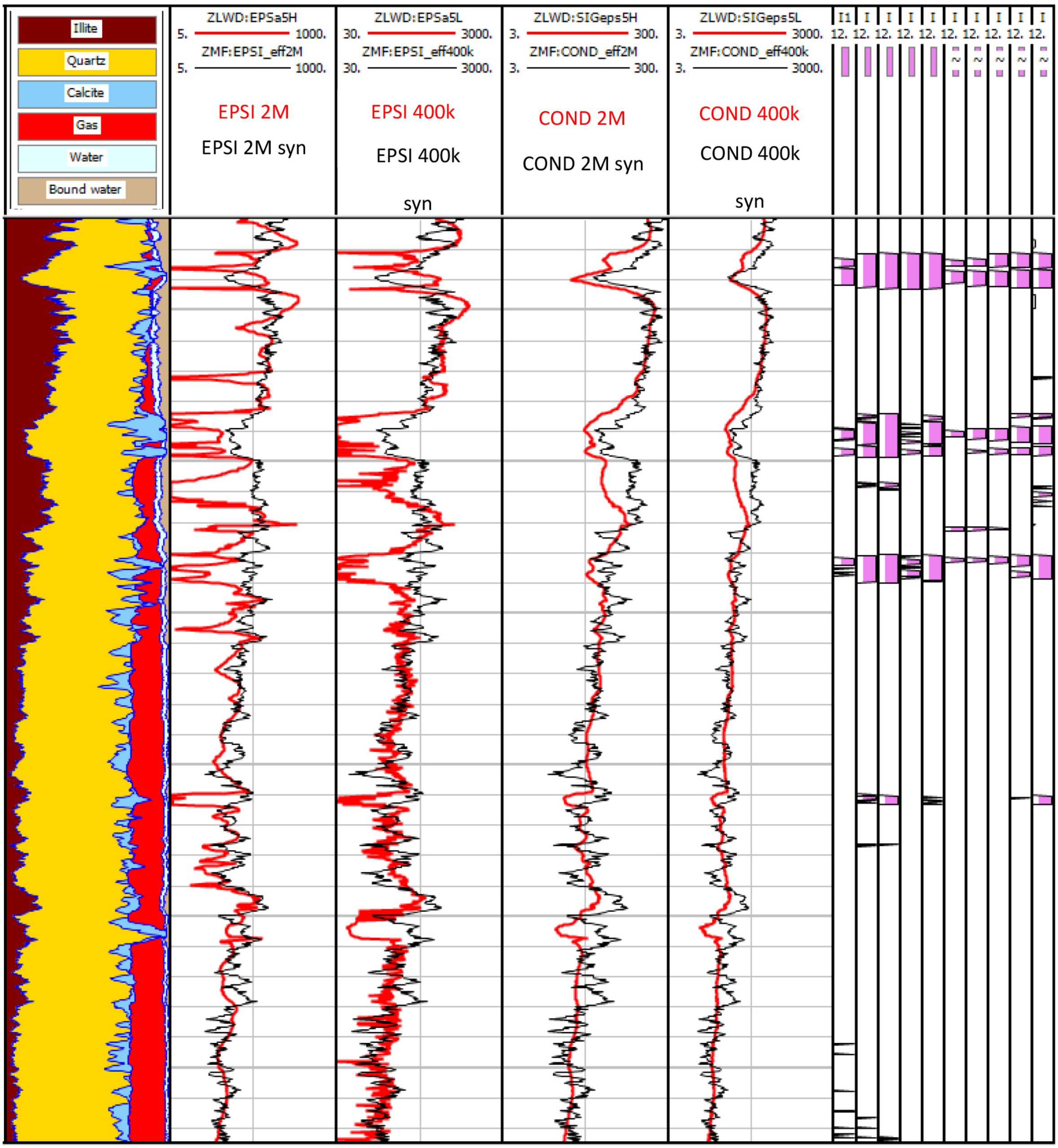

Figure 6. Well #4; high porosity shaly sand deviated well. Track 1 is petrophysical volume analysis which is input to dielectric property modeling. Red curves are outputs of the LWD tool dielectric inversion, permittivity, and conductivity at 400kHz and 2 MHz. Black curves ("syn") are corresponding simulated results. Both the dielectric inversion and the dielectric property model cross- validate each other via the final petrophysical analysis, adjusted to produce the reconciliation of the simulated and actual EM properties.

contrasts between adjacent beds.

Our new, optimized LWD dielectric inversion, while based on previously published work, is a new process. As such, we actually validate both it and the PS model at 400 kHz and 2 MHz simultaneously. Figure 6 is a section of example Well #4. This is a deviated well in a higher porosity shaly sand environment. The associated LWD nuclear log data was input to the PS model to simulate the 2 MHz and 400 kHz permittivity and conductivity curves. Plotting these against the inverted curves shows very good reconciliation at these frequencies, as has been seen at both induction and dielectric tool frequencies.

In cases of discrepancy there may be other electromagnetic effects hidden in the petrophysics, which affect the measurements and thus the convergence behavior of the algorithm. If the formation under investigation features additional petrophysical properties, such as anisotropy or proximity to high-contrast bed boundaries, the algorithm may not converge. In this case, the algorithm is terminated after ten iterations, providing a log- quality-control flag, which indicates that the mathematical and physical assumptions of the inversion algorithms may not be valid and must be generalized to anisotropic media or media with high-contrast stratifications. For example, lamination anisotropy in deviated wells will distort the attenuation and phase-shift measurements in a sense opposite to the dielectric-permittivity distortion of the measurements. In figure 5 there are ten separate tracks at the right side of the log graphic for, in the case of this particular tool, the five tool spacings and two frequencies each of which with its own LQC flag. This results in distortion of the permittivity values, compared to those values simulated by the PS model as seen at the intervals where the LQC flags are triggered.

However, given that we understand the limitations of the process, we assert that we have cross-validated both the LWD dielectric inversion and the PS model-based dielectric property modeling via the actual formation dielectric properties and the associated petrophysical formation analysis serving as the ground truth. The simulation and inversion offer a two-way process, which validates the measurement and ensures their consistency. It also validates the assumption of a homogeneous and isotropic medium.

RESULTS

Wideband Dielectric Property Modeling: N. American Unconventional Shale

We have demonstrated confidence in both modeling and inversion via our methodology, but we do not have LWD propagation tool data in unconventional formations in our test data base. Therefore we have focused on an unconventional source rock WL data set in a vertical well in a North American shale gas reservoir, Well #5.

The WL log data in this well includes array laterolog and array dielectric log measurements, as well as geochemical tool log measurements. As is the typical mode of operation in pilot holes in unconventional resource development, there was no LWD resistivity acquired. The WL geochemical data is very crucial in substantiating the correct fractions of the various complex matrix minerals and fluids present in unconventional mudrocks such as this formation. The PS model simulation based on these volumetric inputs and the other associated formation parameters generated synthetic permittivity and conductivity curves at laterolog, induction, and dielectric

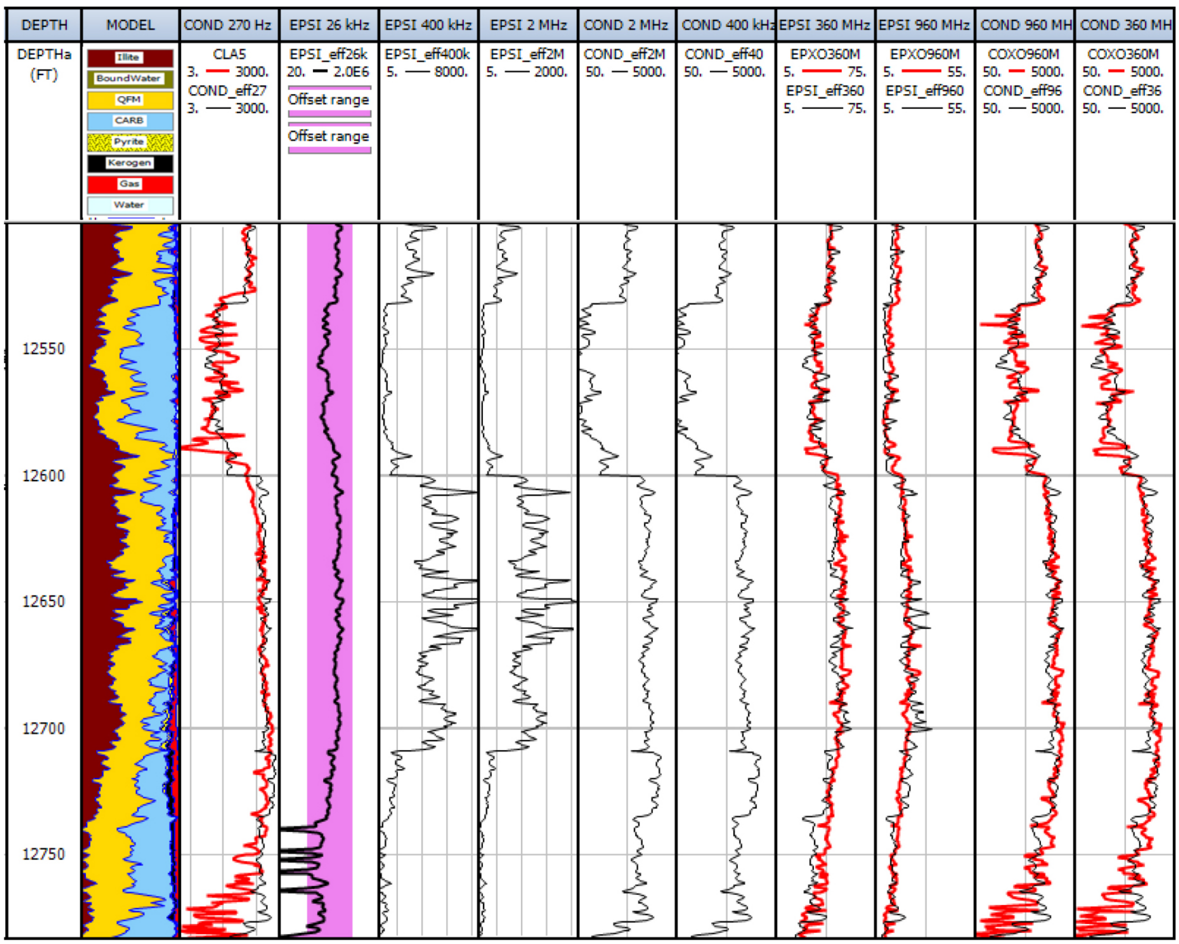

Figure 7 – Well #5. North American gas shale pilot hole wideband simulation, reconstructing actual data. Simulated curves are black, actual data cures are red. Track 3 is reconstruction of array laterolog deepest array conductivity by simulated conductivity at laterolog frequency. Track 4 is simulated permittivity at induction (26 kHz) frequency against a range of inverted permittivities from offset actual induction tool data which is shaded in violet. Tracks 5-8 are simulated permittivity and conductivity curves at LWD (400 kHz, 2 MHz) frequencies. Tracks 9-12 are array dielectric permittivity and conductivity simulated curves at 360 MHz and 960 MHz frequencies reconstructing the actual associated data in the well.

tool frequencies, and at the desired LWD propagation tool frequencies of 2 MHz and 400 kHz.

For ground truth, high-frequency permittivity and conductivity data are direct outputs of the dielectric tool acquisition as usual. There was no induction data in this exact well, but there were near and far offset well data sets which included induction logs, and this data had been previously inverted. For the array laterolog data, no inversion processes are developed presently. However we can use the 270 Hz conductivity simulation from the PS model to compare to the array laterolog conductivity log data as a benchmark. Figure 7 shows the log graphic of the well actual and simulated data. The PS model simulation adjustments were based on reconstructing the 3 highest array dielectric frequency permittivity and conductivities, the array laterolog 270 Hz conductivity, and keeping the induction 26kHz permittivity values within the range of values seen from the actual induction inversions from the offset wells (seen by the green shading in the log graphic). We also make mention of the fact that the organic kerogen in this well is actually over-mature which has caused a certain fraction of it to be graphitized. Thus we observe a very low array laterolog resistivity/high conductivity. Interestingly also, this is quite similar to resistivity log observations seen in Vaca Muerta wells where magmatic intrusions have caused premature maturation and graphitization of organic materials in isolated intervals across the basin.

With reconstruction across the wideband effected, we confidently assert that the simulated 2 MHz and 400kHz permittivities and conductivities would reasonably approximate those which would be seen had there been LWD propagation data in this well which was subsequently inverted for the formation EM properties at these frequencies. Thus we have a wideband dielectric dispersion characteristic for this formation at this well's location.

We have inspected and done petrophysical analysis on a number of data sets in vertical Vaca Muerta wells with a variety of WL EM tools, from laterolog to induction to dielectric devices. We add these to our experience base of performing similar work in several different North American gas shales. This is done in the interest of simulating what would be approximate permittivity and conductivity properties that would be obtained from inversion of actual LWD resistivity tool field logs and associated parameters drive our Dielectric Property Modeling. Most of the data sets contain WL induction data, in which case we perform point-by-point inversion for permittivity and conductivity at induction frequencies to benchmark the low-frequency end of the simulated dielectric properties. If the data s*et al*so contained dielectric tool logs, we use these dielectric values for high frequency calibration points of the simulated dielectric properties.

Wideband Dielectric Dispersion Characteristics: Vaca Muerta Unconventional Shale

We can now investigate specific dispersion characteristics in a lower Vaca Muerta section of a vertical well, Well #6. This is shown in figure 8. A complete petrophysical analysis was completed for input into the dielectric property modeling. The point-by-point induction dielectric inversion for permittivity and conductivity at 26 kHz is shown as red points in tracks 3 and 4 along with the associated dielectric property modeling simulation as black curves.

These are the low frequency validation. Tracks 9 – 14 show the array dielectric tool field permittivity and conductivity curves at 108 MHz, 360 MHz. and 960 MHz as red curves, and the corresponding simulated quantities as black curves as the high-frequency validation. Based on the adjusted petrophysical volumes and parameters that resulted in acceptable reconstruction at both the low- and high-frequency ends of the wideband spectrum, we can simultaneously simulate permittivity and conductivity curves at the LWD frequencies of 400 kHz and 2 MHz, seen as black curves in tracks 5-8 with light blue shading. This then provides the wideband EM dispersion characteristic for this section of the Vaca Muerta formation in this well and at this point in the reservoir.

Following the methodology of Wang and Poppitt, 2013, we select some discrete points in the reservoir to plot the dispersion characteristic more clearly. In a preliminary attempt to relate these to critical formation properties, we extract Vclay from the petrophysical analysis at these points, as seen in figure 9. And, as Wang and Poppitt observed, we see a change in the dispersion behavior as a function of Vclay. Further we calculate the slope of the dispersion for the permittivities at LWD frequencies (green arrows in fig. 9) only, M_{LWD}. And we note that the for the change in clay volume from 10.4% to 25.9%, the slope become about 5 times (negatively) steeper: -1.88 e-4 to -3.88 e-5.

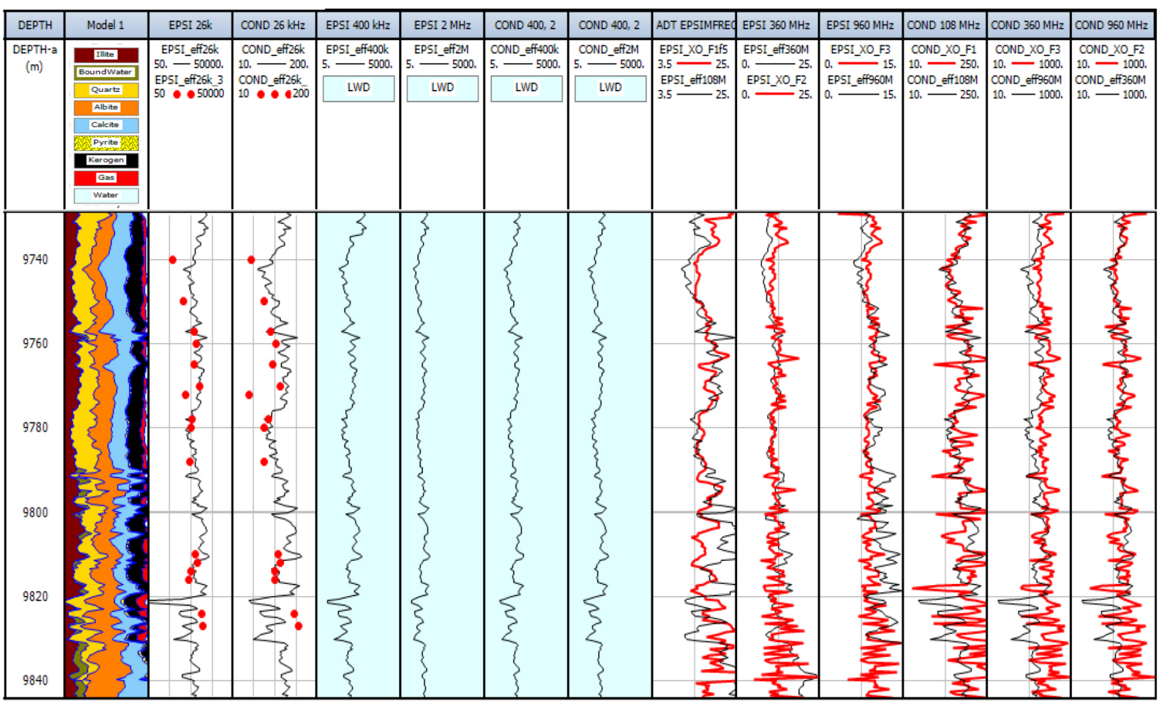

Figure 8. Vaca Muerta intervals in Well #6. Black curves are simulated permittivity and conductivity curves at induction (26 kHz), LWD (400 kHz, 2 MHz - blue shading) and array dielectric (108 MHz, 360 MHz, and 960 MHz) frequencies benchmarked to induction inversion points (red dots) and array dielectric field data (red curves).

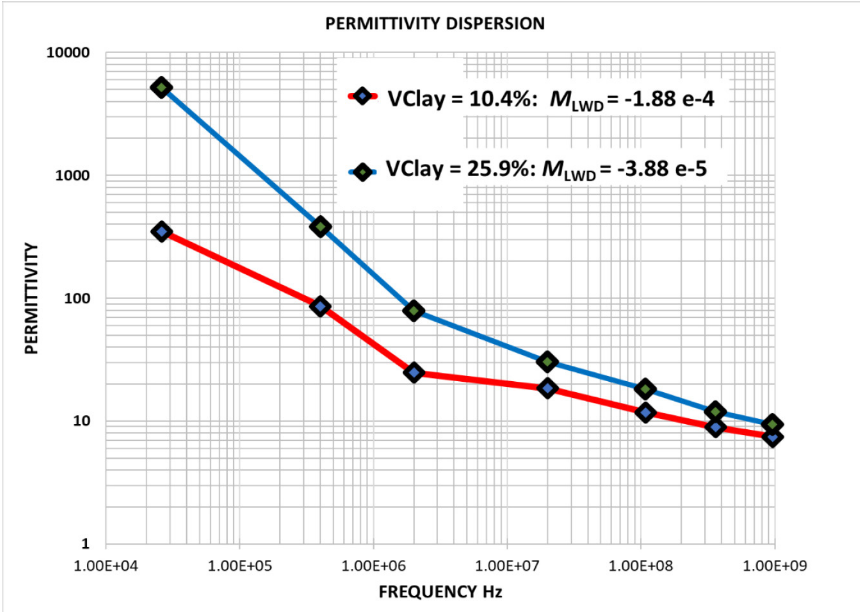

Figure 9. Wideband dielectric dispersion characteristics for discrete points in Well # 6. The clay volume at these two depth points has a good range of values from 25.5 % to 10.4%. The overall dispersion characteristic is distinctly different, and the slope of the LWD frequency dispersion alone is about 5 times steeper at the higher clay volume.

At this point we are still in the early stages of matching these types of dispersion sensitivities to petrophysical and formation properties, but we are encouraged that this not only mirrors the findings of Wang and Poppitt, 2013, but it also begs the very important question of whether dielectric dispersion inverted from LWD acquisition alone can be related to key information about formation producibility, especially in horizontal production drainholes in unconventional mudrocks reservoirs, like Vaca Muerta.

Simulation of LWD Dielectric Dispersion Characteristics: Unconventional Shale Lateral well

We return to Well #5 seen in figure 7. Based on the model validation in that particular formation at both the high and low- frequency ends of the dispersion spectrum, we would like to simulate the LWD dielectric properties of a typical lateral well with a target trajectory in the "sweet spot" of the source rock formation seen in the vertical well, considering it as the pilot hole.

This is actually the case given by the Well #1 lateral trajectory in figure 1, where the well is shown to have wider variations in stage-by-stage gas production. The lateral was landed in a similar formation as that in Well #5, with less kerogen maturity and so with no graphitization. However Well #1 was also logged with a modern cased-hole pulsed-neutron spectroscopy device, which was then interpreted for formation volumetrics to be input into our dielectric property modeling.

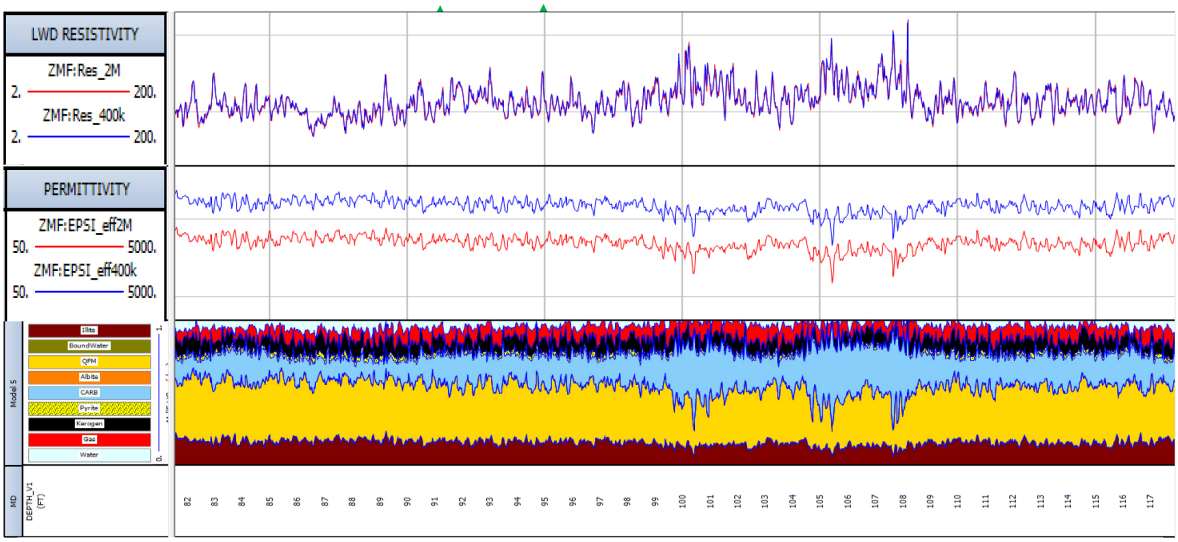

Figure 10. Section of Well #1 lateral log data. Track 2 is volumetric analysis from a CH pulsed neutron geochemical tool. Track 3 is dielectric property model simulation of LWD frequency permittivities (blue curve: 400kHz, red curve: 2 MHz). Track 4 is associated inverted conductivities at LWD frequencies converted to resistivities. (blue curve: 400kHz, red curve: 2 MHz).

Figure 10 is a log display of the CH log-derived formation evaluation in Track 2 and the simulated LWD frequency permittivities at 400 kHz and 2 MHz in Track 3. Track 4 contains the simulated LWD frequency conductivities converted to resistivities at the same frequencies.

We now insert these simulated quantities into the log display format of figure 1 as an illustration or prediction of what could have been derived had the wells actually been acquiring LWD propagation resistivity tool data – and subsequently inverted with our dielectric inversion process while drilling. This is now seen in figures 11a,

b. The resulting data display would include the TVD/ trajectory in Track 1, GR in Track 2, measured depth in Track 3, and the inverted permittivity and conductivity / resistivity logs, as seen above in figure 10, in Tracks 4 and 5.

Additionally, we have taken some preliminary steps of interpretation of these “LWD-only” quantities. Referring to the wideband and then validated 400kHz – 2MHz dispersion sensitivity to Vclay that we described above in our Vaca Muerta well analysis, we calculate that LWD dispersion quantity, EPSI_DISP_LWD, seen in Track 6, in this well and then do a simple Vclay derivation in the same fashion as what would be done with a GR curve – to wit, pick the EPSI_DISP_LWD minimum and maximum log points and scale the curve linearly between these endpoints to generate a “VCLLWD” curve. Track 7 compares VCLLWD curve to a typical GR- only Vclay curve, VCLGR, derived from the log data in the same fashion.

The violet shading indicates when it is seen that the GR-based clay volumes are over-estimated compared with the dielectric dispersion quantities. This is a plausible condition as the typical GR measurement in organic rich mudrocks is dominated by the presence of uranium that exists in large amounts in these formations, and thus is an unreliable source of clay volume information.

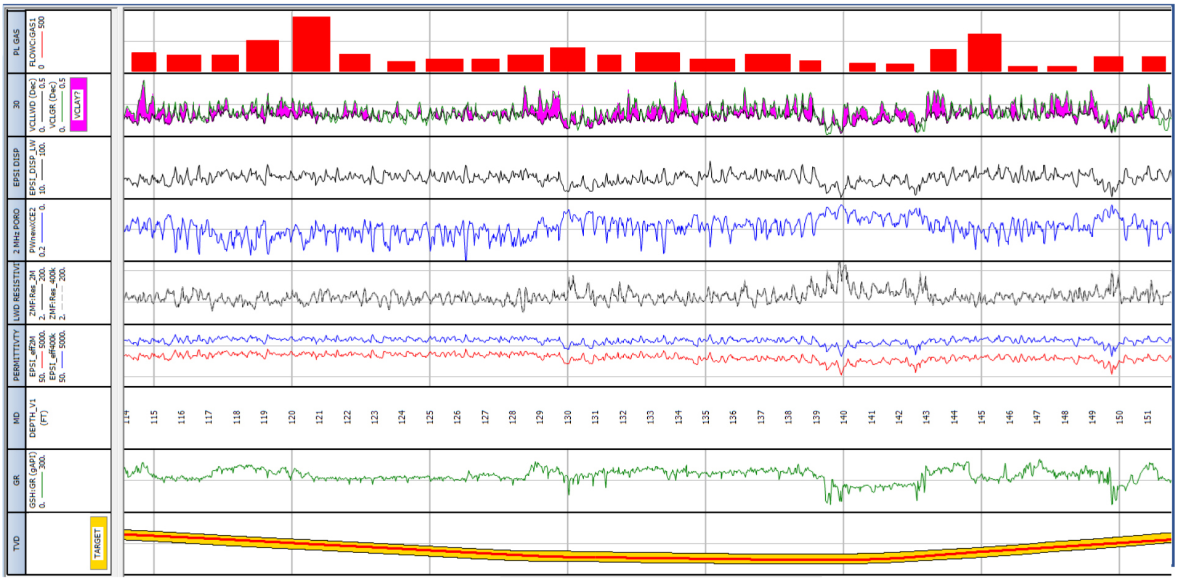

Figure 11a– Section of Well #1 lateral log data with added simulated LWD inversion outputs and calculations. Track 1 is the well trajectory (red curve) in TVD against the target layer in gold shading. Track 2 is MWD GR. Track 3 is measured depth. Track 4 is dielectric property model simulation of LWD frequency permittivities (blue curve: 400kHz, red curve: 2 MHz). Track 4 is associated inverted conductivities at LWD frequencies converted to resistivities. (blue curve: 400kHz, red curve: 2 MHz). Track 5 is calculated permittivity dispersion, “EPSI_DIFF LWD”. Track 6 is VClay calculated from permittivity dispersion (“VCLLWD”) and VClay calculated from MWD GR “VCLGR”, with shading to highlight VCLLWD > VCLGR. Track 7 is an adaptive salinity-independent water-filled porosity from 2 MHz permittivity (“PW2M”). Track 8 is gas flow rate per stage from production log interpretation.

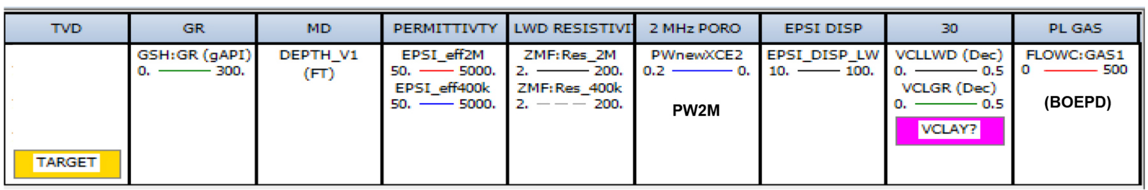

Figure 11 b. Curve insert header for log in Figure 11a.

To complete our current and early-stage interpretation processes from LWD dielectric inversion, Track 8 displays a provisory, adaptive, 2 MHz “dielectric” porosity curve. As seen in Jacobsen, Bartenhagen, *et al.*, (2022), this is a salinity-independent, water-filled porosity quantity. It would be compared to total porosity from e.g., a nuclear log interpretation, to allow the derivation of water saturation without the need for knowledge of water-resistivity, Rw.

The final track in figure 11a shows again the variable Well #1 stage-by-stage gas production, perplexing as it is given the fact that Track 1 confirms that the wellbore is in the target sweet-spot of the reservoir. Does this production correlate at all to any of the new dielectric properties and subsequent interpreted quantities?

We wish to postulate that there is much more information pertaining to formation attributes that must still be extracted from LWD frequency permittivity and conductivity and the associated dispersion of these quantities in this particular range of the wideband EM tool spectrum. We do know that there is some overlap of dielectric polarization mechanisms in this band (Anderson *et al.*, 2007), and that all of these phenomena are dependent on the physical, microscopic fabric of porous rock. It is our firm belief that further investigation into these mechanisms, supported by the re-analysis of both existing, legacy LWD propagation resistivity tool data and of future LWD data in new laterals, will net more insight into how unconventional laterals respond to completion and treatment practices. And the end result of this will be improved and more cost-effective development of unconventional shale resource reservoirs.

CONCLUSIONS AND RECOMMENDATIONS

We have implemented a process to perform dielectric property modeling across the frequency range of EM resistivity/dielectric logging devices in the industry today. The PS model takes petrophysical analysis volumetric inputs and other key formation parameters. The simulation has been validated against high- frequency , mid-frequency (LWD) and low-frequency properties inverted from raw data acquired at these frequencies.

We have implemented a point-by-point inversion for dielectric formation properties from low-frequency (induction) tool data which is validated against dielectric property modeling.

We have implemented an improved inversion for dielectric formation properties of mid-frequency (LWD) axisymmetric resistivity propagation tool data which is accurate, efficient, vendor agnostic, and validated against dielectric property modeling

We have performed a wideband inversion for Vaca Muerta dielectric formation properties in wells with induction and array dielectric data.

We have simulated LWD frequency (400kHz, 2 MHz) Vaca Muerta dielectric formation properties and have found correlations of permittivity dispersion to clay volume throughout the Vaca Muerta stratigraphic column.

We have reason to believe that dielectric dispersion characteristics are sensitive to the microscopic fabric of both mudrocks as well as conventional formations. And that this sensitivity is manifest at wideband and subsets of if for different polarization phenomena. We feel that the LWD frequency range in particular has not been studied in enough depth to understand these sensitivities and that critical reservoir properties which impact well productivity directly are as yet underived completely.

We urge the petrophysical community to review and re-analyze existing, legacy LWD propagation resistivity tool data sets in the light of the findings in this paper. This is especially valid in the Vaca Muerta formation if such data has been acquired in any of the production lateral wells that are increasingly being drilled. This could present a new opportunity to utilize these long wellbores to characterize the reservoir much more extensively along the length of the whole lateral, and the vertical/volumetric section which it drains.

NOMENCLATURE

Abbreviations

ADT = Array Dielectric Tool

AT = tool measurement of signal attenuation

CEC = cation exchange capacity

CLA5 = Conductivity of array laterolog tool deepest array (= 1 / RLA5), (mS/m)

$COND_{eff270}$ = conductivity at 270 Hz simulated from PS model, (mS/m)

$COND_{eff26k}$ = conductivity at 26 kHz simulated from PS model, (mS/m)

$COND_{eff26k_{39}}$ = conductivity at 26 kHz from induction tool inversion of 39" spacing signal, (mS/m)

$COND_{eff400k}$ = conductivity at 400 kHz simulated from PS model, (mS/m)

$COND_{eff2M}$ = conductivity at 2 MHz simulated from PS model, (mS/m)

$COND_{eff360M}$ = conductivity at 360 MHz simulated from PS model, (mS/m)

$COND_{eff960M}$ = conductivity at 360 MHz simulated from PS model, (mS/m)

$COND_{H_{40}}$ = inverted 2 MHz conductivity, 40" spacing, (mS/m)

$COND_{L_{40}}$ = inverted 400 kHz conductivity, 40" spacing, (mS/m)

COXO360M = conductivity at 360 MHz from ADT tool, (mS/m)

COXO960M = conductivity at 960 MHz from ADT tool, (mS/m)

EM = electromagnetic

$EPSI_{eff26k}$ = permittivity at 26 kHz simulated from PS model, dimensionless

$EPSI_{eff26k_{39}}$ = permittivity at 26 kHz from induction tool inversion of 39" spacing signal, dimensionless

$EPSI_{eff400k}$ = permittivity at 400 kHz simulated from PS model, dimensionless

$EPSI_{eff2M}$ = permittivity at 2 MHz simulated from PS model, dimensionless

$EPSI_{eff360M}$ = permittivity at 360 MHz simulated from PS model, dimensionless

$EPSI_{eff960M}$ = permittivity at 960 MHz simulated from PS model, dimensionless

EPSa5H = inverted 2 MHz permittivity, deepest tool spacing (e.g., 40"), dimensionless

EPSIa5L = inverted 400 kHz permittivity, deepest tool spacing (e.g., 40"), dimensionless

EPT= electromagnetic propagation tool

EPXO360M = permittivity at 360 MHz from ADT tool, dimensionless

EPXO960M = permittivity at 960 MHz from ADT tool, dimensionless

I2H = dimension indicator diagnostic, high-frequency, 40"spacing

I2L = dimension indicator diagnostic – low-frequency, 40" spacing

LWD = logging while drilling

NMR = nuclear magnetic resonance PhiT= total porosity

PS = geoelectromagnetic effective medium model

PS = tool measurement of signal phase

PW2M = water-filled porosity from 2 MHz permittivity

QC = quality control

RAT = attenuation resistivity curve

RESat5H = raw, field log 2 MHz attenuation resistivity, deepest tool spacing (e.g., 40"), (Ohm-m)

RESeps5H = inverted 2 MHz resistivity, deepest tool spacing (e.g., 40"), (inverse of $COND_{H40}$) (Ohm-m)

RESps5H = raw, field log 2 MHz phase shift resistivity, deepest tool spacing (e.g., 40"), (Ohm-m)

Rw = resistivity of connate formation wate

RPS = phase resistivity curve

SIG = special interest group

WL = wireline

Symbols

σ_a = formation conductivity, S/m
σ^* = complex formation conductivity, S/m
ε_a = formation permittivity (or dielectric constant), dimensionless
ε^* = complex formation permittivity (or dielectric constant), dimensionless

REFERENCES

Altman, R., B. I. Anderson, M. G. Lüling, J. Rasmus, 2008, "Dielectric Effects and Resistivity Dispersion on Induction and Propagation-Resistivity Logs in Complex Volcanic Lithologies: A Case Study", SPWLA 49th

Annual Logging Symposium, (2008), paper JJJJ.

Anderson, B. I., Barber, T. D., Lüling, M. G., Sen, P., 2006, "Observations of Large Dielectric Effects on Induction Logs, or, Can Source Rocks Be Detected with Induction Measurements?", SPWLA 47th Annual Logging Symposium, (2006), paper OOO

Anderson, B. I., Barber, T. D., Lüling, M. G., Sen, P., Taherian, M. R., Klein, J., 2008, "Identifying Potential Gas-Producing Shales from Large Dielectric Permittivities Measured by Induction Quadrature Signals", SPWLA 49th Annual Logging Symposium, (2008), paper HHHH.

Anderson, B. I., Barber, T. D., Lüling, M. G., Rasmus,J., Sen, P. N., Tabanou, J. R., Haugland, M., 2007, Observations of Large Dielectric Effects on LWD Propagation-Resistivity Logs, paper BB, SPWLA 48th Annual Logging Symposium, Austin, TX, USA, June 3-16.

Anderson, B.I., Shray, F., Hemingway, J., Decoster, E., Swinburne, P. R., Jacobsen, S. J., 2022, "Dielectric Inversion of LWD Propagation-Resistivity Tools for Formation Evaluation", SPWLA 63rd Annual Logging Symposium, Stavanger, Norway, June 10-15.

Chadwick, C., Whittaker, C., 2011, Production Logging Challenges in Horizontal Shale Gas Wells, paper H, SPWLA 52nd Annual Logging Symposium, May 14–18, 2011.

Clark, B. O., Lüling, M. G., Jundt, J., Ross, M., 1990, "Well Logging Apparatus And Method For Determining Formation Resistivity At A Shallow And A Deep Depth", US patent US 4,899,112, 1990.

Clark, B. O., Lüling, M. G. , Jundt, J., Ross, M., Best, D., 1988, "A Dual Depth Resistivity Measurement for FEWD [Formation Evaluation While Drilling]", SPWLA 29th Annual Logging Symposium, (1988), paper A.

Illfelder, H. M. J., Badea, E. A., Boonen, P., Zhipeng Liu, 2008, Identification of Formation Fluids Using the Dielectric Constant Determined from LWD Wave Propagation Measurements", paper ZZZ, SPWLA 49th Annual Logging Symposium (2008).

Jacobsen, S. J., Bartenhagen, K., Anderson, B. I., Shray, F., Hemingway, J., Decoster, E., Swinburne, P. R., 2022, Deep Salinity-Independent Water Saturation from Low-Frequency Dielectric Rock Properties, SPWLA 63rd Annual Logging Symposium, Stavanger, Norway, June 10-15.

Jacobsen, S. J., Decoster, E., Hemingway, J., Shray, F., Anderson, B. I., Swinburne, P. R., 2022, "Formation Permittivity and Conductivity Simulation from Petrophysical Volumetric analysis, SPWLA 63rd Annual Logging Symposium, Stavanger, Norway, June 10-15.

Jin, Y., Misra, S., Homan, D., 2020, Estimation of In-Situ Wettability Using Multi-Frequency Electromagnetic Measurements, Paper URTeC: 2928, presented at the Unconventional Resources Technology Conference, Austin, TX, USA, July 20-22.

Lüling, M. G. , 2014, "Simultaneous inversion of induction data for dielectric permittivity and electric conductivity", US patent US 8,694,259B2, 8 Apr. 2014.

Misra, S., Rasmus, J., Homan, D. M., Lüling, M. G., Barber, T. D., 2016, "Dielectric Effects in Pyrite-rich Clays on Multifrequency Induction Logs and Equivalent Laboratory Core Measurements", SPWLA 57th Annual Logging Symposium (2016), paper Z.

Norbisrath, J. H., 2018, Dielectric Permeability Logging, paper J, SPWLA 59th Annual Logging Symposium, London, UK, June 2-6.

Norbisrath, J. H., Grammar, G. M., Vanden Berg, B., Tenaglia, M., Eberli, G. P., Weger, R. J., 2017, Nanopore Imaging in Vaca Muerta Mudrocks to Evaluate Controls on Complex Resistivity Spectra in Unconventional Reservoirs. SPE-185167-PA, Society of Petroleum Engineers, SPE Res Eval & Eng. 20 (04): 1028-1044.

Rasmus, J. C., Kenyon, W. E., 1985, An improved Petro-physical Evaluation of Oomoldic Lansing-Kansas city Formations Utilizing Conductivity and Dielectric Log Measurements, paper V, SPWLA 26th Annual Logging Symposium (1985).

Stalheim, S. O., 2019, Deducting Dispersive Permittivity from LWD Resistivity Measurements, paper VVVV, SPWLA 60th Annual Logging Symposium, The Woodlands, TX, USA, June 17-19.

Wang, H., Poppitt, A., 2013, The Broadband Electromagnetic Dispersion Logging Data in a Gas Shale Formation, paper AA, SPWLA 54th Annual Logging Symposium, New Orleans, LA, USA, June 22-26.